5. Trapping with static fields

Atoms in Magnetic Field

Breit Rabi Formula for F=I+1/2

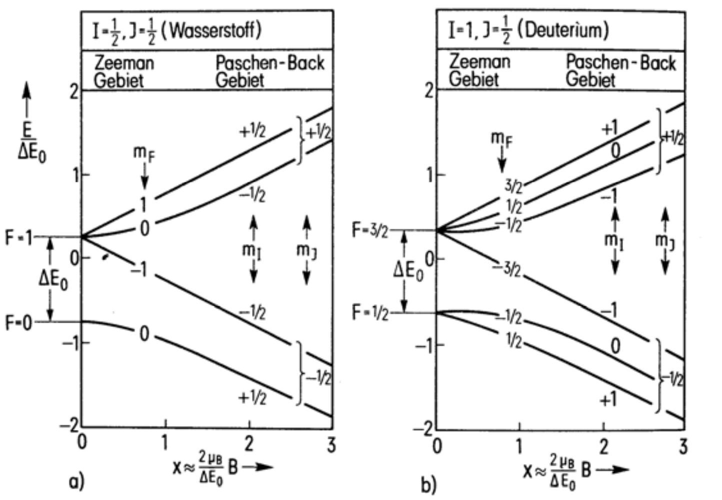

Fig. 102 Feldabhängigkeit der HFS-Aufspaltung nach der Breit-Rabi-Formel für I = 1/2 und I = 1

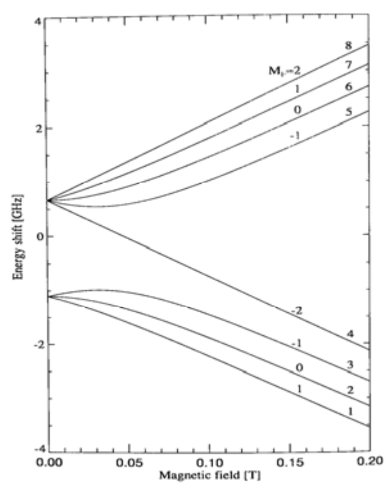

FIGURE 4.2. Energies of the ground hyperfine states of Na, where the states are numbered 1–8 and M_F is the projection of the total angular momentum of the atom on the magnetic field axis.

$$E_B^{HFS}(F = I \pm \tfrac{1}{2}, m_F) = -\frac{A}{4} + m_F g_K \mu_K B \pm \frac{\Delta E_0}{2}\sqrt{1 + \frac{4m_F}{2I+1}x + x^2}$$

$$x = \frac{g_J \mu_B - g_K \mu_K}{\Delta E_0} \approx \frac{2\mu_B}{\Delta E_0} \qquad \Delta E_0 = A(I + \tfrac{1}{2})$$

No Trapping Theorems

- **Earnshaw's theorem:**
  It is impossible to arrange any set of charges to generate point of stable equilibrium in a charge free region.
- **Optical Earnshaw's theorem:**
  If the light scattering force is proportional to the local Pointing vector, it is impossible to construct an optical trap.
- **No field maximum theorem:**
  In regions free of charges and currents |E| and |B| cannot have a local maximum.
- **No compensation theorem:**
  No combination of static electric, magnetic and/or gravitational fields can produce a stable atom trap.

Magnetic Trapping

$$\text{Trapping potential: } U_{mag} = -\vec{\mu}\cdot\vec{B}$$

$$\text{for } \mu = \mu_B: \quad 1\,\text{Gauss} \rightarrow U_{mag} = 67\,\mu\text{K} = 5.78\times10^{-9}\ \text{eV}$$

Magnetic states:

$U_{mag} < 0$ high field seeking (attracted to maximum)
$U_{mag} > 0$ low field seeking (attracted to minimum)

Earnshaw Theorem:

No maximum of a static field (combination of fields) in a source free region

Magnetic traps are low field seeker traps,

Atoms trapped in minimum of field
but not in the ground state of potential
(this would be a high field seeking state)

Avoid Zeros in the field (Majorana transitions)

Quadrupole trap has a zero in the field at the centre !
Even at non zero weak field, there are Landau-Zener transitions possible.

Rate for a harmonic minimum: $\gamma = \frac{\pi\omega}{2\sqrt{e}}\, e^{\frac{-\mu_{\|} B_{ip}}{\hbar\omega}}$

B_{ip} ... field at minimum
ω ... trap frequency

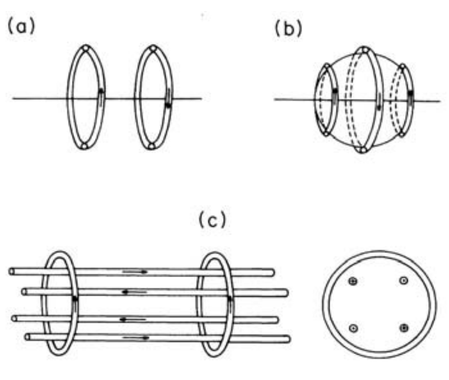

FIG. 1. Three magnetostatic trap configurations discussed in this work. (a) The magnetic quadrupole trap, consisting of two coils with opposing currents. (b) The "spherical hexapole" trap, with three wires on the surface of a sphere. With equal currents and the outer coils at 45°, B=0 at the origin. (c) The Ioffe trap, which has a bias field and axial confinement from a two-coil "bottle field" and transverse confinement from a four-wire quadrupole focusing field. Both side and end views are shown for the Ioffe trap.

quadrupole hexapole

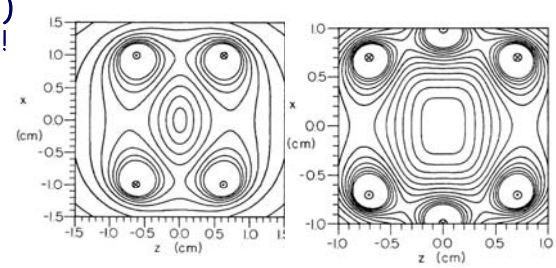

Avoiding the Magnetic Field Zero

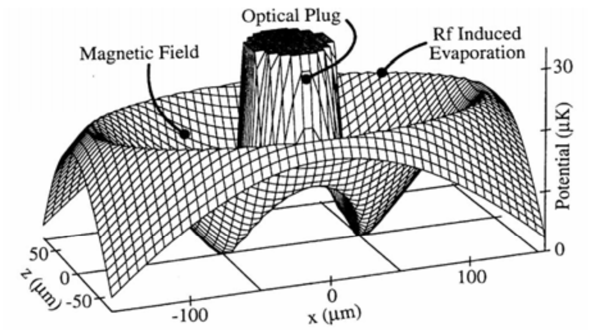

FIG. 1. Adiabatic potential due to the magnetic quadrupole field, the optical plug, and the rf. This cut of the three-dimensional potential is orthogonal to the propagation direction (y) of the blue-detuned laser. The symmetry axis of the quadrupole field is the z axis.

Time Orbiting Potential trap

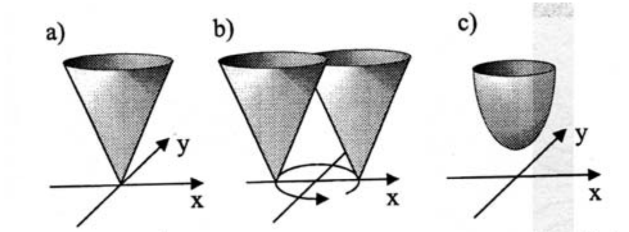

Abbildung 3.4: *Funktionsprinzip einer TOP-Falle. Das lineare Potential a) wird durch das homogene Feld in Rotation versetzt b). Zeitgemittelt ergibt sich in erster Näherung das in c) gezeigte harmonische Potential.*

Configurations with non-Zero Field Minimum

Clover Leaf Trap (MIT)

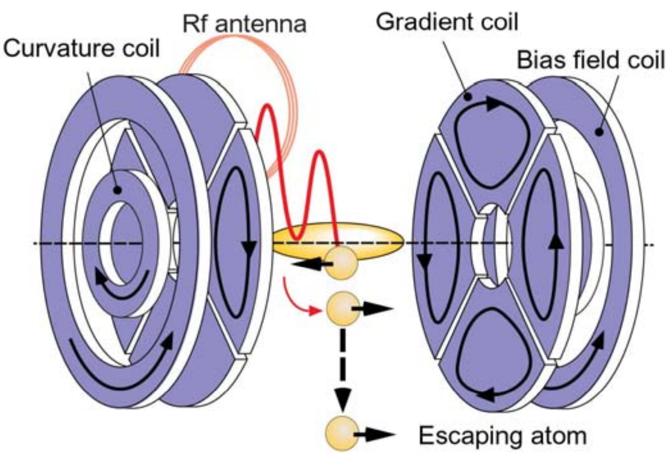

Fig. 4. – In a cloverleaf trap, Ioffe bars are replaced by eight "cloverleaf" coils surrounding the pinch coils, providing 360 degree optical access. Evaporation is done by selectively spin-flipping atoms into untrapped states with rf radiation.

Ioffe Pritchard Trap

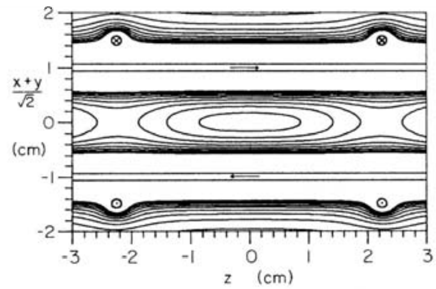

FIG. 7. Contours of $|\mathbf{B}|$ for the Ioffe trap of Fig. 1(c) in the plane of the straight wires. The four straight wires lie on a circle of radius 1 cm, the coils of radius 1.5 cm are spaced by 4.5 cm, and all currents are 100 A. The minimum field at the origin is 14.3 G. Contours are shown at 10 G intervals up to 100 G.

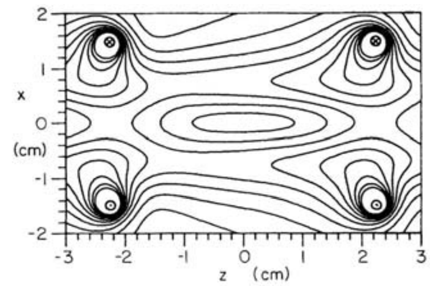

FIG. 8. Contours of $|\mathbf{B}|$ at 10 G intervals to 100 G in a plane midway between the straight wires for the Ioffe trap with parameters as given in Fig. 7. For a plane perpendicular to the one chosen, the contours will be as shown, but reflected in the $z=0$ line.

Tailoring magnetic fields for compression

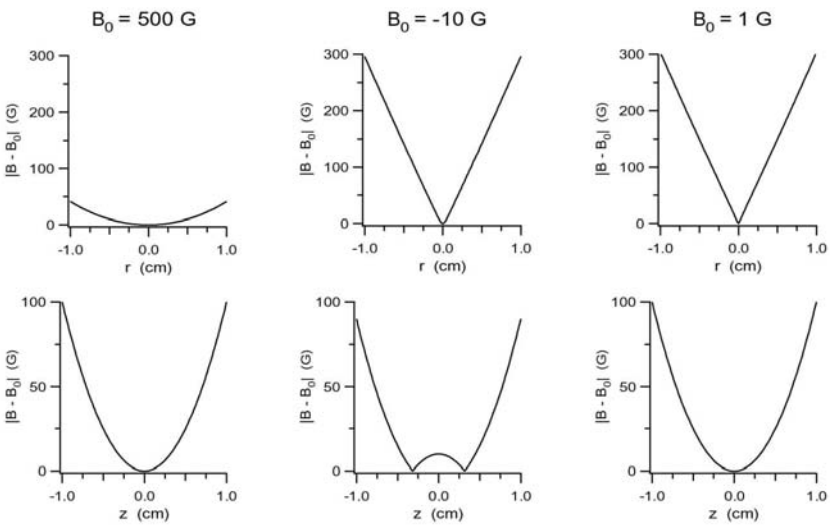

Fig. 3. – Bias field compensation in an Ioffe-Pritchard trap is important for tight radial confinement. The magnetic field in an IP trap characterized by a radial gradient of 300 G/cm and an axial curvature of 200 G/cm^2 is shown for three bias fields B_0. The upper row displays radial cuts, and the lower row displays axial cuts of the magnetic field profile. In the first column, radial confinement is softened as a result of the large bias field. In the second column, the bias field is over-compensated, resulting in a pair of zero field crossings along the axis of the trap. In the third column, the bias field is tuned correctly, resulting in tight radial confinement and no zero field crossings.

Baseball Trap
(JILA)

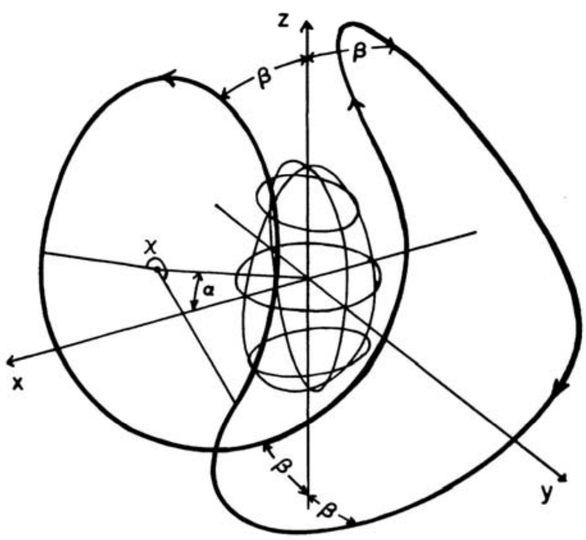

FIG. 9. The baseball coil (heavy line) with an equipotential surface shown schematically at the center. The coil consists of four contiguous planar circular segments, each subtending an angle χ, on axes at angle $\alpha(-\alpha)$ with respect to the $\pm x$ ($\pm y$) directions. At closest approach, the coil comes within angle β of the z axis. For this figure, $\alpha = 20°$ (hence $\beta = 21.6°$), and the contour lines represent a 40-G surface for a baseball of radius $R_B = 1$ cm, current $I_B = 100$ A.

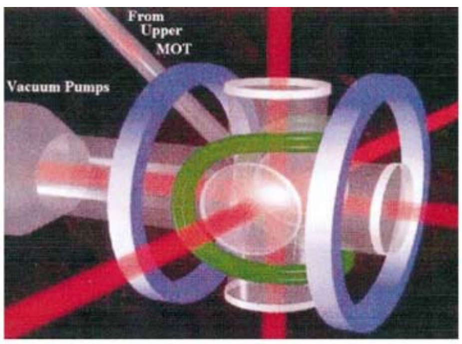

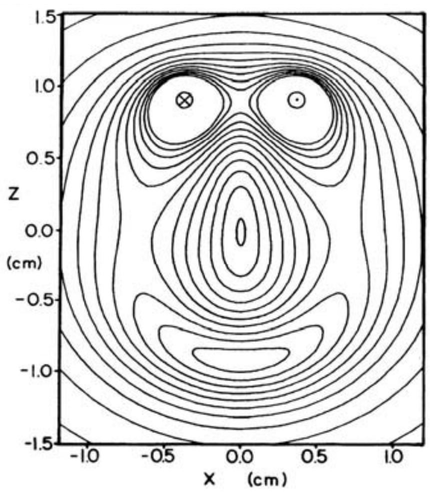

FIG. 10. Contours of $|\mathbf{B}|$ in the x-z plane of Fig. 9, with $\alpha = 20°$ $R_B = 1$ cm, and $I_B = 100$ A. Contours are drawn at 10-G intervals. At the center, $|\mathbf{B}|_{min} = 9.1$ G, while the transverse and axial saddle-point thresholds are 72 and 106 G, respectively.

Quic Trap
(LMU, ENS)

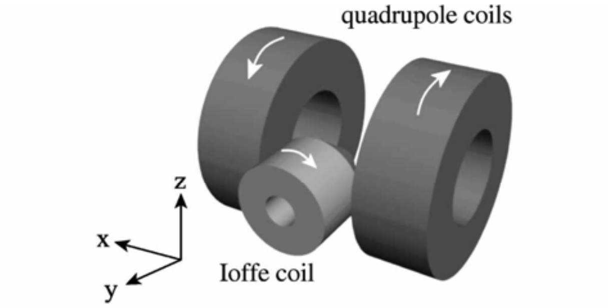

FIG. 1. QUIC trap: The Ioffe coil converts the spherical quadrupole trap into an Ioffe trap with its trap center close to the Ioffe coil. No additional coils are needed to produce a bias field. The arrows indicate the direction of the current flowing through the coils.

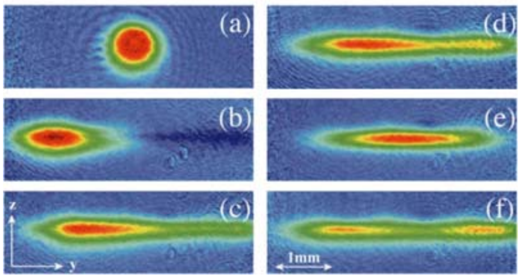

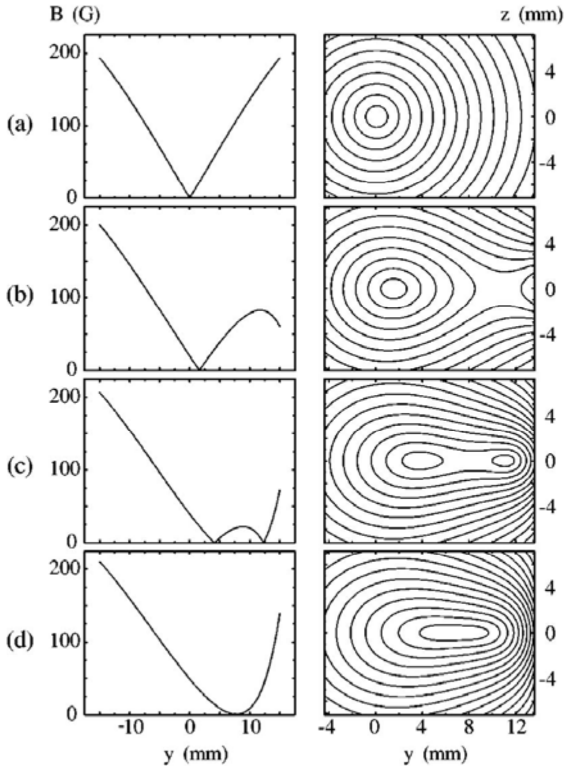

Magnetic Transport

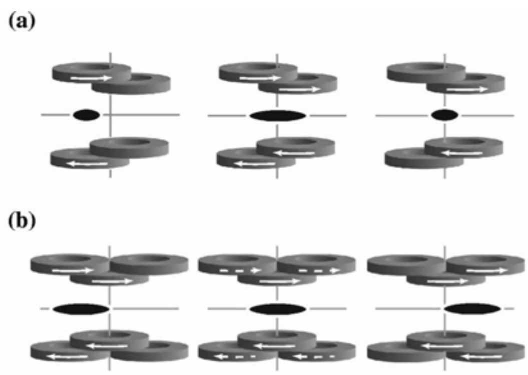

FIG. 2. Schematic setup for the transfer of a magnetic quadrupole trapping potential. The solid and dashed arrows indicate the current direction and strength. (a) By increasing the current in the second quadrupole coil pair and afterwards decreasing the current in the first quadrupole coil pair, the trapping potential may be moved. Here the aspect ratio is changed during the transport process. (b) By running suitable currents through three quadrupole coil pairs it is possible to maintain a constant aspect ratio during the transport process.

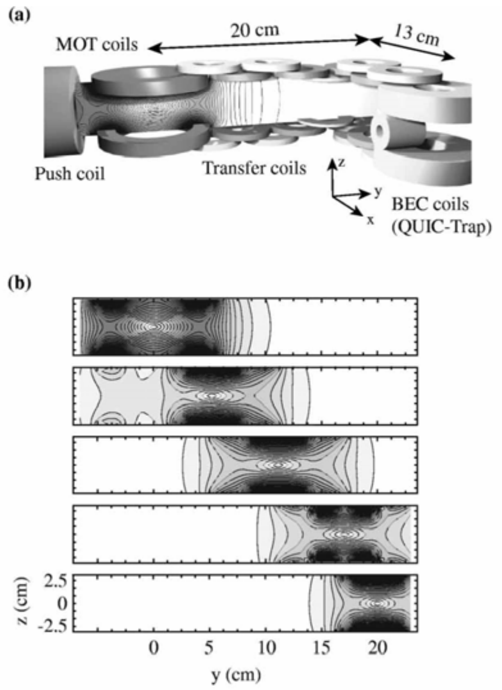

FIG. 1. (a) Experimental setup of the quadrupole coil pairs for the transport process. The magnetic trapping potential is moved over 33 cm around a 90° corner into an UHV vacuum region of a glass cell. (b) Contour plots, showing the absolute value of the magnetic field during different stages of the first half of the transport sequence.

Micro Traps

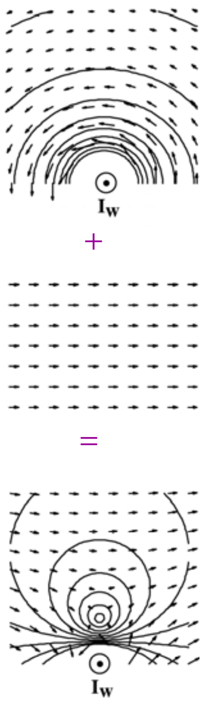

Trapping field is created by super-position of the field of a current carrying wire and a homogeneous bias field

Potential
- **depth:** bias field
- **minimum:** angle current<-> field
- **gradient:** $1/I$

Mount wire on a surface:
Use nanofabrication to build mesoscopic structures

How to build a trap

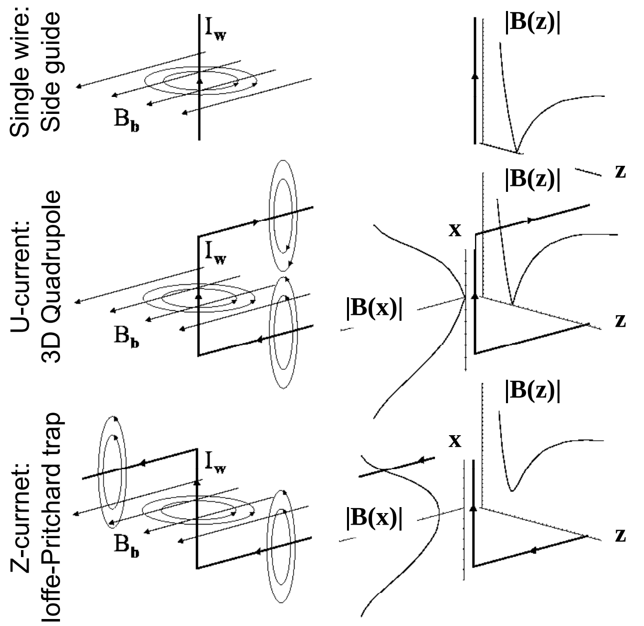

Z-Wire Trap (Innsbruck)

Paul Trap
RF trap

Equation of motion:
(Mathieu equation)

$$m\frac{d^2u}{dt^2} + [a_u - 2q_u\cos(\Omega t)]u = 0$$

where u represents the x, y and z coordinates, and a_u and q_u are dimensionless trapping parameters.

$$a_x = \frac{8eU}{mr_0^2\Omega^2}$$
$$q_x = -\frac{4eV}{mr_0^2\Omega^2}.$$
$$a_z = -\frac{8eU}{mr_0^2\Omega^2}$$
$$q_z = \frac{4eV}{mr_0^2\Omega^2}.$$

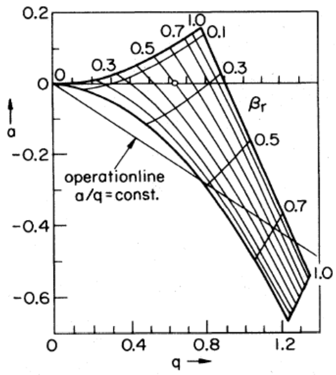

Mass spectrometers
Precision spectroscopy
Clocks
Quantum information

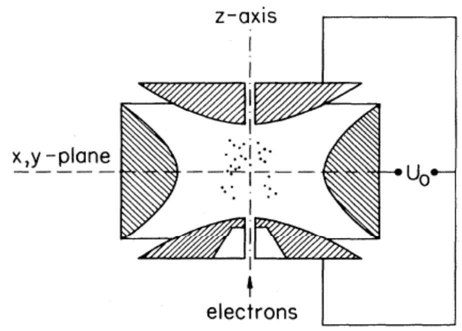

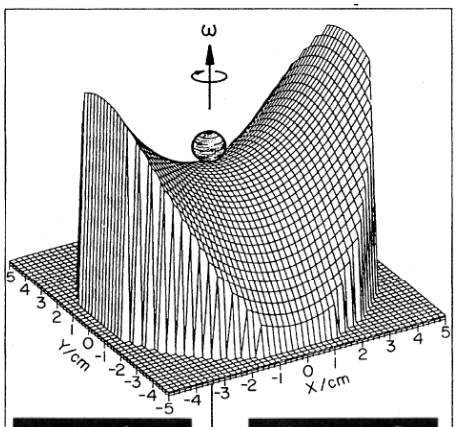

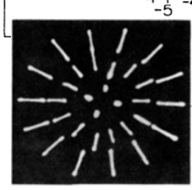

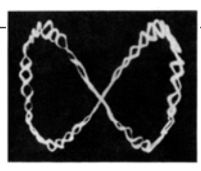

Penning Trap

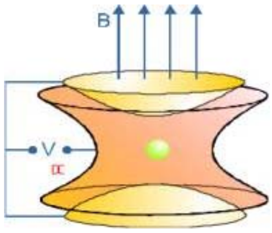

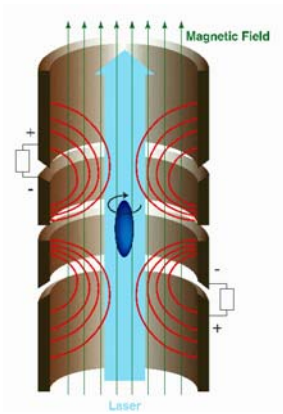

Cyclotron oscillation: $\omega_+ = \frac{\omega_c}{2} + \sqrt{\frac{\omega_c^2}{4} - \frac{\omega_z^2}{2}} \approx \omega_c - \frac{\omega_z^2}{2\omega_c}$

Axial oscillation: $\omega_z = \sqrt{\frac{1}{m}\frac{\partial^2 E_{\text{pot}}}{\partial z^2}(0)} = \sqrt{\frac{q}{m}\frac{C_2 V_0}{d^2}}$

Magnetron oscillation: $\omega_- = \frac{\omega_c}{2} - \sqrt{\frac{\omega_c^2}{4} - \frac{\omega_z^2}{2}} \approx \frac{\omega_z^2}{2\omega_c}$

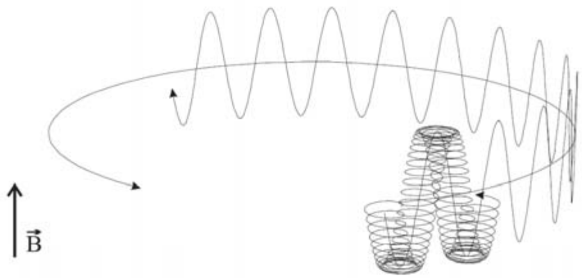

$$\omega_c^2 = \omega_+^2 + \omega_z^2 + \omega_-^2$$

$\omega_c = \frac{q}{m} B_z$ mass, magnetic moments (g-2) $\hbar\omega_L = -\mu B = -g m_S \mu_B B$

5.2 Evaporative cooling to BEC

BEC
the basics

$$\frac{1}{e^{(E-\mu)/k_BT}} = Ae^{-\frac{E}{k_BT}}$$ classical particles Maxwell-Boltzmann statistics

$$P(E) = \begin{cases} \dfrac{1}{e^{(E-\mu)/k_BT}-1} & \mu < 0 \\[2ex] \dfrac{1}{e^{(E-\mu)/k_BT}+1} & \mu = E_F \end{cases}$$

Bosons Bose-Einstein statistics ($\mu < 0$)

Fermions Fermi-Dirac statistics ($\mu = E_F$)

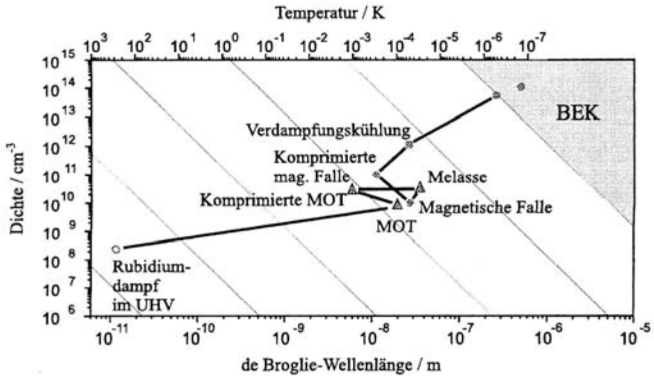

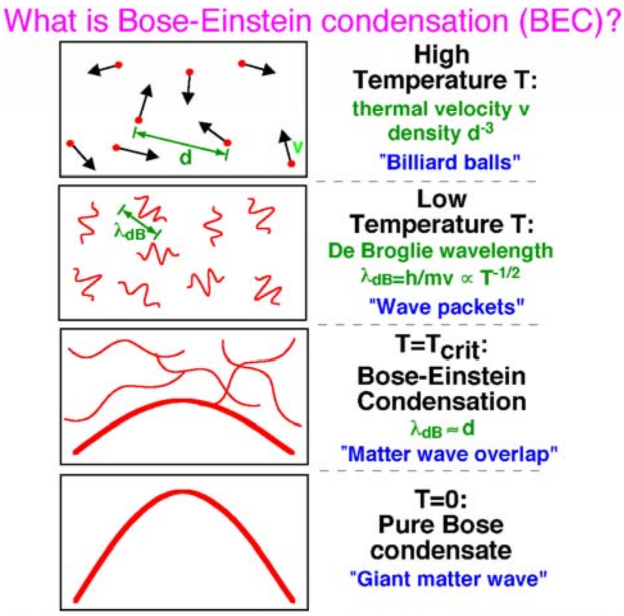

Two indistinguishable Particles

Wave function for 1 Particle $\psi(x_1)$

Wave function for 2 Particles $\psi(x_1, x_2)$

We can only observe $|\psi(x_1, x_2)|^2$

If the particles are indistinguishable we find: $|\psi(x_1, x_2)|^2 = |\psi(x_2, x_1)|^2$

There are 2 possibilities:

Boson : $\psi_+(x_1, x_2)$: $\psi_+(x_1, x_2) = +\psi_+(x_2, x_1)$

$$\psi_+(x_1, x_2) = \frac{1}{\sqrt{2}}[\psi_1(x_1)\psi_2(x_2) + \psi_2(x_1)\psi_1(x_2)]$$

Fermion $\psi_-(x_1, x_2)$: $\psi_-(x_1, x_2) = -\psi_-(x_2, x_1)$

$$\psi_-(x_1, x_2) = \frac{1}{\sqrt{2}}[\psi_1(x_1)\psi_2(x_2) - \psi_2(x_1)\psi_1(x_2)]$$

Two indistinguishable Particles II

sets see what happens if the two particles are at the same location (state)
that is if $x_1 = x_2$

$\psi_+(x_1, x_1) \neq 0 \rightarrow$ Bosons can occupy the same state

$\psi_-(x_1, x_1) = 0 \rightarrow$ Fermions can not occupy the same state

consequently for 2 Bosons at the same location (in the same state) we find:

$$|\psi(x,x)|^2 = 2\,|\psi_1(x)\psi_2(x)|^2$$

probabilities to find n particles in the same state:

n classical particles $\quad P_n = (P_1)^n$

n Bosons $\quad P_n^{Boson} = n!(P_1)^n$

probability to add another Boson to a state with n Bosons

$$P_{n+1}^{Boson} = (n+1)P_1 P_n^{Boson}$$

stimulated scattering, stimulated emission

Cooling in a Conservative Trap
evaporative cooling

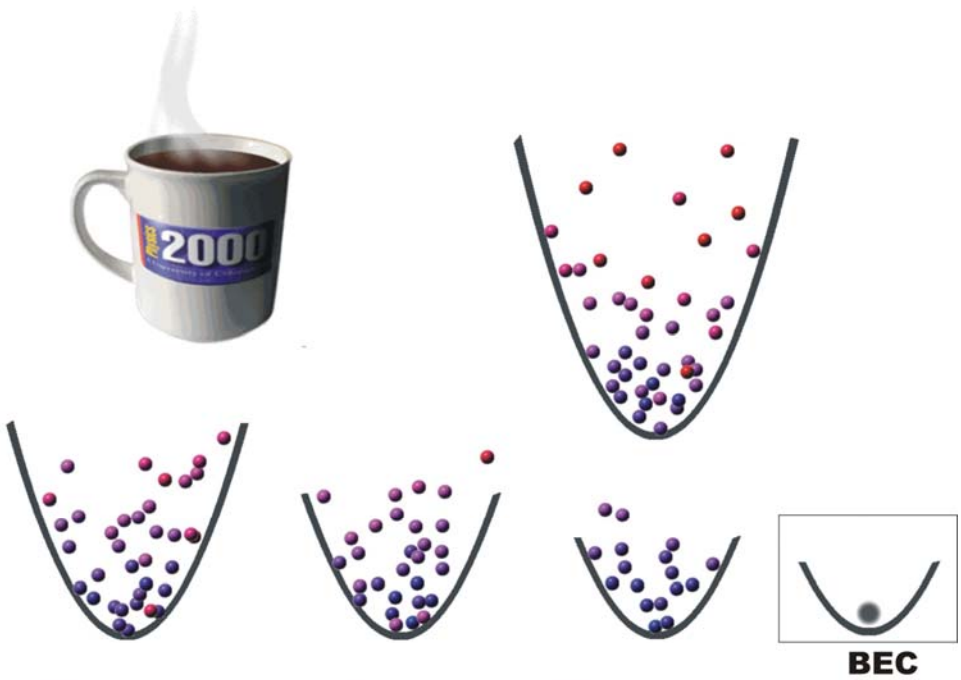

http://www.Colorado.EDU/physics/2000/bec/

Evaporative Cooling

H.F. Hess Phys.Rev.B 34 p R3476 (1986)
K.B. Davis, M-O. Mewes, W. Ketterle Appl.Phys.B 60, p155 (1995)
O.J.Luiten, M. Reynolds, J. Walraven Phys.Rev.A 53 p381 (1996)

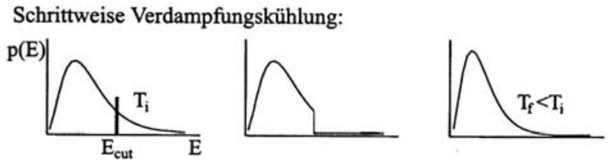

General Scaling

Evaporative cooling happens at exponential scale
Time scale is given by the thermalisation (collision) time
(it takes about 5 collision for a truncated distribution to thermalise)
Characteristic quantities are logarithmic derivatives
A key parameter is $\alpha = \frac{d(\ln T)}{d(\ln N)}$ (temperature decrease per particle loss)
Evaporation is controlled by a potential depth ηkT

The density of states ($\rho(\varepsilon)$) of trap pot. determines scaling.
For power law potentials: $\rho(\varepsilon)=A_{pl}\,\varepsilon^{1/2+\delta}$
square well: $\delta=0$, harmonic: $\delta=3/2$, linear: $\delta=3$

Ioffe-Pritchard trap: $\rho(\varepsilon)=A_{IP}\,(\varepsilon^3+2U_{IP}\,\varepsilon^2)$

Exponential scaling for a d-dimensional potential $U(r) \sim r^{d/\delta}$

Number of atoms N	1	with: $\alpha = \frac{d(\ln T)}{d(\ln N)} = \frac{\eta+\kappa}{\delta+\frac{3}{2}} - 1$
Temperature T	α	
Volume V	$\alpha\delta$	
Density n	$1-\alpha\delta$	average energy in potential
Phase space density D	$1-\alpha(\delta+3/2)$	$\langle\varepsilon\rangle = (\delta+3/2)\,kT$
Elastic coll. Rate $n\sigma v$	$1-\alpha(\delta-1/2)$	

Run-away evaporation:

Achieve faster and faster thermalsation with cooling
Collision rate has to grow: $\alpha(\delta-1/2)>1$

Collisions:
good collisions: elastic collisions
bad collisions: inelastic coll., trap loss coll., etc … limit the trap lifetime

How many collisions per tapping time for run away evap.?
Linear trap: > 25 collisions per lifetime
Harmonic trap >150 collisions per lifetime

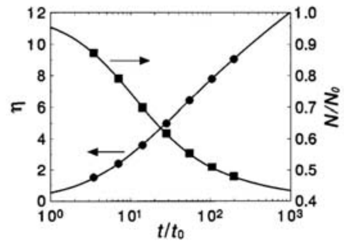

FIG. 5. Truncation parameter η (circles) and fraction of atoms remaining in trap N/N_0 (squares) as a function of reduced time t/t_0 after initiating evaporation from infinite temperature. Curves are obtained by integration of the differential equations resulting from the truncated Boltzmann approximation, symbols by fitting to the distribution obtained by numerical solution of the kinetic equation.

RF induced evaporation

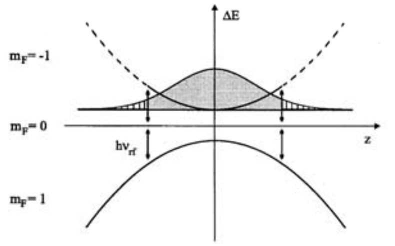

Abbildung 3.11: *Radiofrequenz-induzierte Verdampfungskühlung in einem magnetischen Potential.*

Evaporative Cooling

experiment

Methods of evaporation

First experiments (Hydrogen):
contact with walls Hess et al. PRL 59, 672 (1987)
Saddle point evaporation Masuhara et al. PRL 61, 935 (1988)

RF induced evaporation
Na Davis et al. PRL 74, 5202 (1995)
Rb Petrich et al. PRL74, 3352 (1995)

Optical traps by lowering the potential
Na Adams et al. PRL 74, 3577 (1995)

Dimensionality of evaporation:

To achieve fast and efficient evaporation the loss mechanism should be open or all directions of motion in the trap
(3-d evaporation)

Lower dimensional evaporation (2-d or 1-d) require effective mixing of the degrees of freedom in the motion inside the trap.

Heating from a shaking trap:

Simple model: $\frac{1}{t_{heat}} = \pi^2 \nu_{trap}^2 S(2\nu_{trap})$

$S(\nu) = \varepsilon^2/\Delta\nu$ is the power spectrum of the fractional field noise ε in a bandwidth $\Delta\nu$
stability of 10^{-3} to 10^{-4} is adequate to achieve BEC

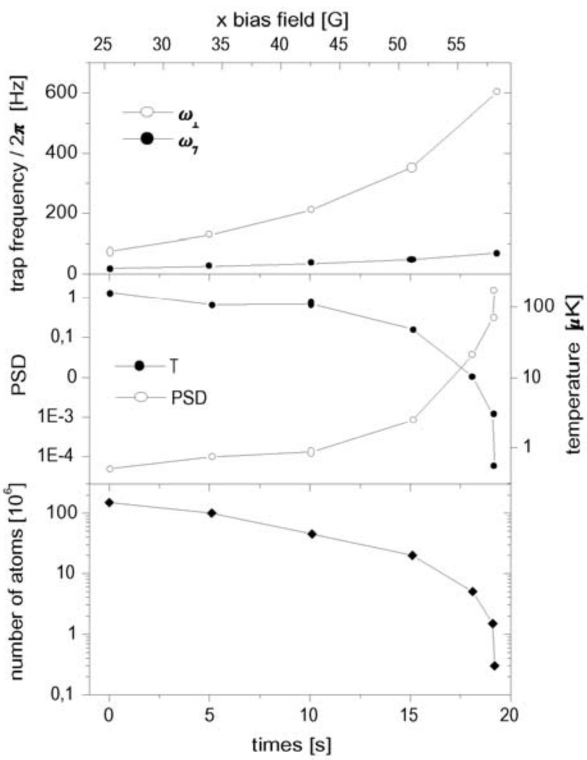

Observing the BEC

Methods of imaging:

3 processes: absorption, emission, shifting the phase
3 methods: absorptive, fluorescence, dispersive imaging
Description: complex index of refraction

$$n_{ref} = 1 + \frac{\sigma_0 n \lambda}{4\pi}\left[\frac{i}{1+\delta^2} - \frac{\delta}{1+\delta^2}\right] \quad \text{with } \delta = \frac{\omega-\omega_0}{\Gamma/2}$$

Transmission T and phase shift Φ

$$T = e^{-\tilde{D}/2} = \exp\left(-\frac{1}{2}\frac{\tilde{n}\sigma_0}{1+\delta^2}\right) \quad \text{with } \tilde{D} = \frac{\tilde{n}\sigma_0}{1+\delta^2}$$

$$\Phi = -\delta\frac{\tilde{D}}{2} = -\frac{\delta}{2}\frac{\tilde{n}\sigma_0}{1+\delta^2}$$

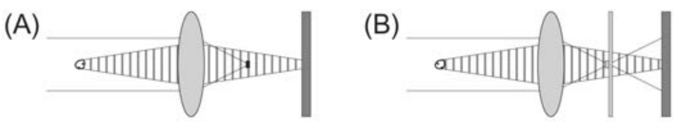

Fig. 7. – Dark-ground (A) and phase-contrast (B) imaging set-up. Probe light from the left is dispersively scattered by the atoms. In the Fourier plane of the lens, the unscattered light is filtered. In dark-ground imaging (A), the unscattered light is blocked, forming a dark-ground image on the camera. In phase-contrast imaging (B), the unscattered light is shifted by a phase plate (consisting of an optical flat with a $\lambda/4$ bump or dimple at the center), causing it to interfere with the scattered light in the image plane.

Imaging dense clouds (D_0>100):

Optimal absorption imaging is at optical density of 1
Need large detuning **but** there is *refraction* at $|\delta|$>0
For diffraction limited imaging we need a phase shift $\Phi < \pi/2$
For optical density 1 we need $|\delta|=(D_0)^{1/2}$
At this detuning the phase shift $\Phi \sim 0.5\,(D_0)^{1/2}$ much too large
For $\Phi < \pi/2$ we need $|\delta|=D_0/\pi$
Need phase contrast imaging

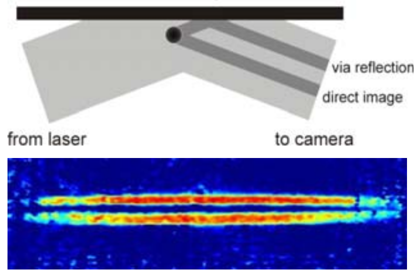

Non destructive imaging:

Example of an image: 30x30 pixel with 100 photons each (10^5 photons)
This can be *'non perturbative'* for large condensates.
Important figure of merit: ratio signal / heating

- **Absorption imaging:** each photon gives one recoil energy
- **Dispersive imaging:** there are more forward scattered photons than absorbed photons
  - for large detuning the gain is $D_0/4$!
  - elastic scattered photons contribute not to heating if imaging is done in the trap and light pulse is longer that $1/\nu_{trap}$
  - one can make many pictures of the condensate
- For low density clouds there is *no* advantage of dispersive imaging

Lens setup (3μm resolution)

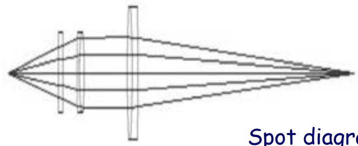

Spot diagram

Wie sieht man die Kondensation

von der Seite

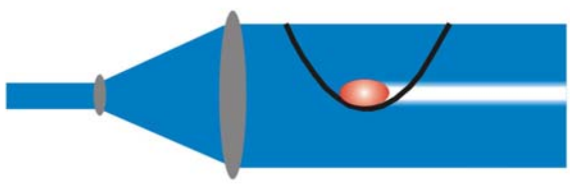

von vorne

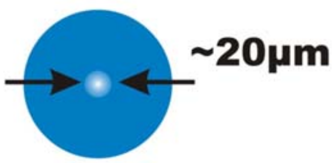

Freie Expansion

thermisch **BEC**

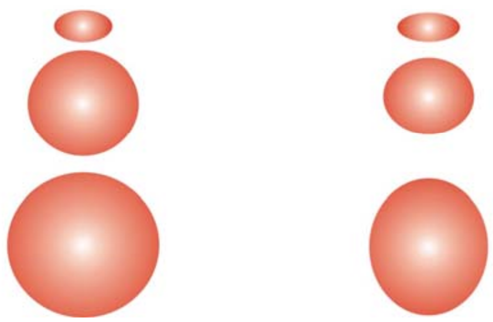

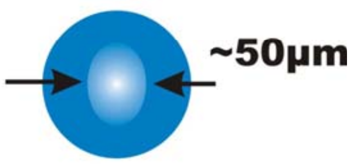

absorption imaging

reference image (I) background image (I_0) devided image

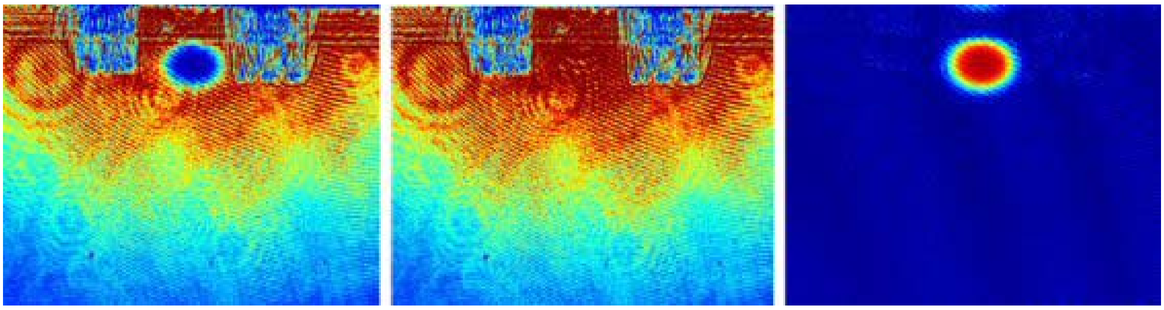

Typical example: an image with 30 x 30 pixels and 100 detected photons/pixel involve 10^5 absorbed photons

Heating: $1E_{rec}$ per photon $\rightarrow$ ejects atom from BEC

absorption imaging is **destructive** for BECs $\leq 10^5$ atoms,

larger BECs can be imaged several times (H-BEC: 10^9 atoms)

A single-atom fluorescence camera

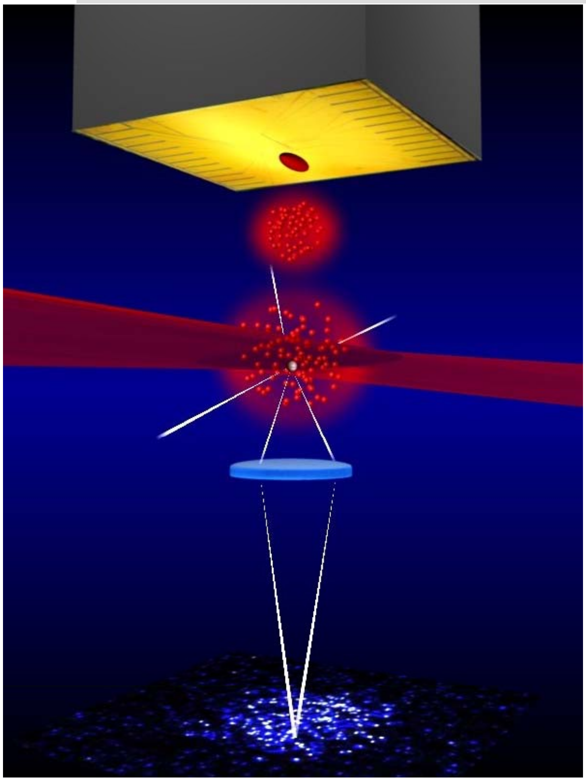

Experimental realization

• Atom cloud is released from **chip trap**

• After 4 – 8 mm fall it passes a thin **sheet of light**:
- two counter-propagating lasers, 20 µm waist
- resonant / detuned from $|5S_{1/2}, F=2\rangle \rightarrow |5P_{3/2}, F=3\rangle$
- in light sheet, each atoms scatters ~ 900 photons

• a **high NA imaging system** captures 20 photons
- numerical aperture 0.34
- depht of field 40 µm (essentially zero background)
- spatial resolution 8 µm over 4 mm diameter

• **intensified (EMCCD) camera** records images
- major noise source: clock induced charges $\cong$ 1 photon

Fluorescence Camera

Single Atom Detection

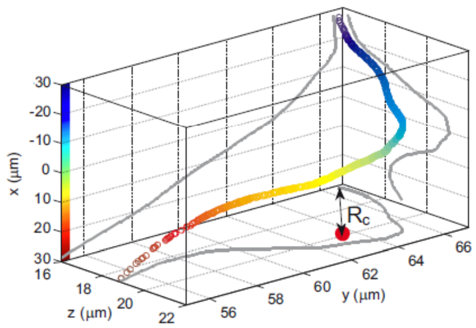

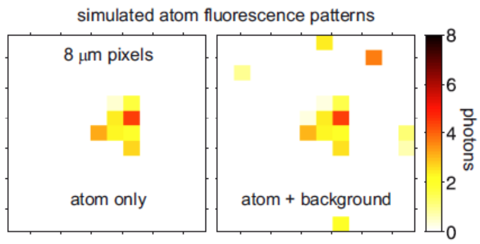

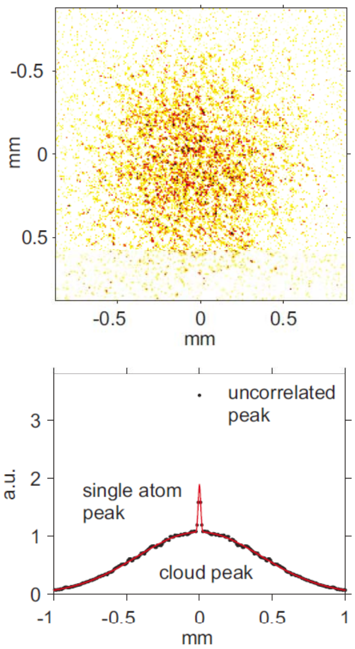

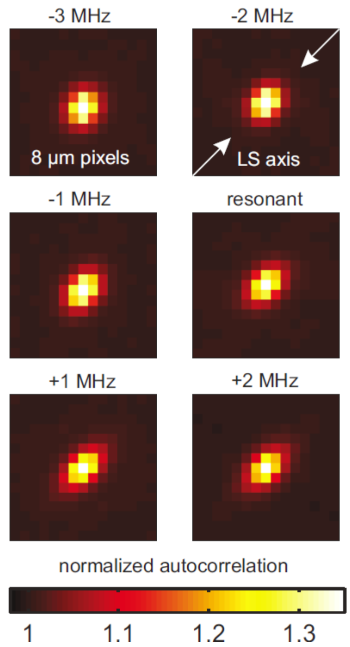

Fluorescence Camera

Large Dynamic Range

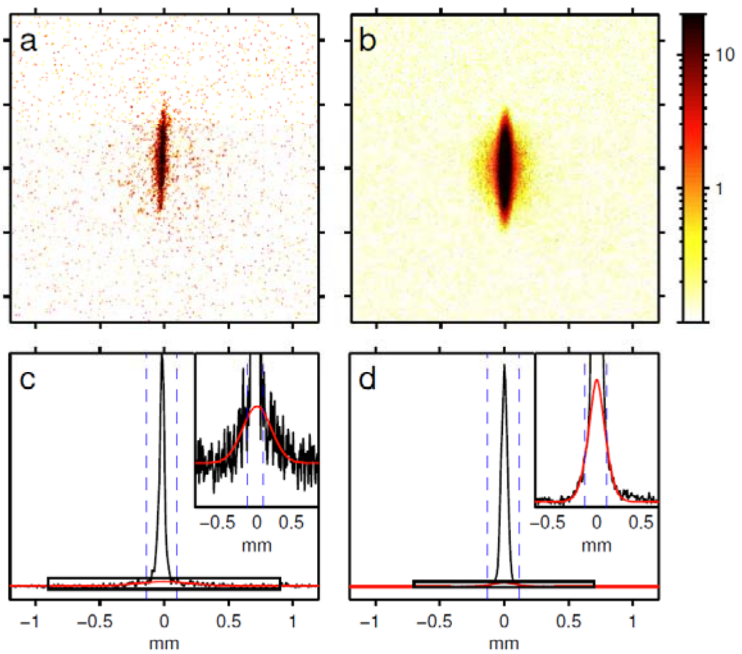

The large dynamic range of the single atom sensitive imaging allows to see very small thermal clouds besides the BEC, and measure very small temperatures T~T_c/10

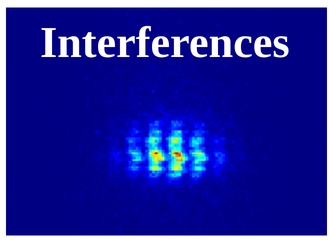

imaging techniques – a comparison

All imaging techniques equally illuminate the atom cloud with a probe beam.
They differ in how much information can be extracted per absorbed photon
$\rightarrow$ figure of merit (ζ)

Best suited imaging:

$$\boxed{\frac{\zeta_{dispersive}}{\zeta_{absorptive}} \approx \frac{D}{4}}$$

- dense clouds/BECs ($D \cong 300$): **dispersive** (phase contrast) **imaging** allows to take up to 100 frames of a single sample (in-situ or short ToF)
- dilute clouds ($D \cong 1$): **absorption imaging** allows to detect down to 10 atoms/μm^2 for long ToFs (problematic when imaging dense clouds)
- single atoms ($D << 1$): in **fluorescence imaging**, the signal/noise ratio is determined by
  - electronic noise (<2 photons /pixel)
  - background light reaching the detector

  single atom detection is possible when reducing background light to 10^{-5}

Remark: single atom detection is **easy** using ionizing / MCP detection ($\rightarrow$ seminar)

Observing BEC

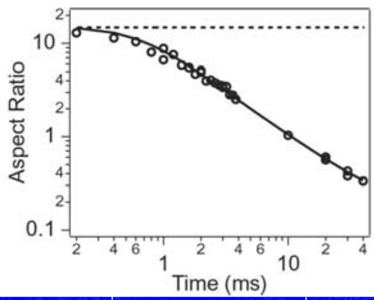

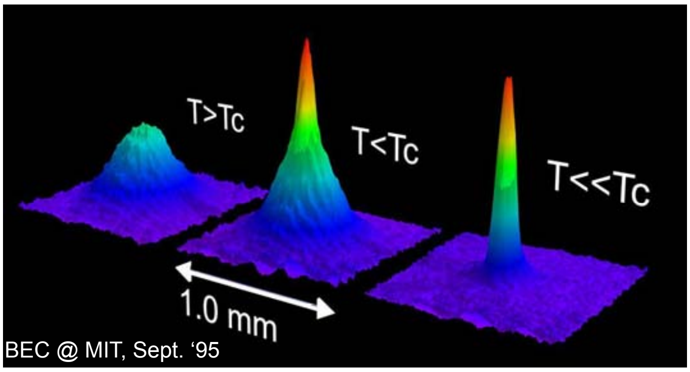

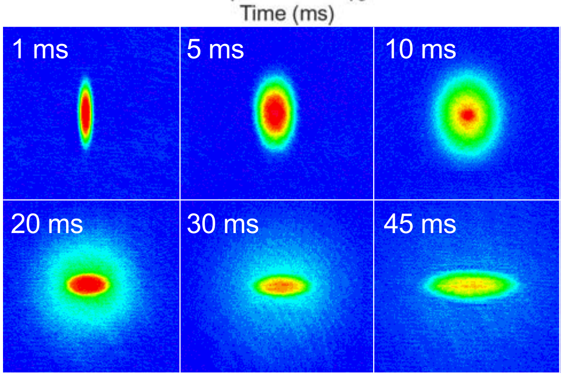

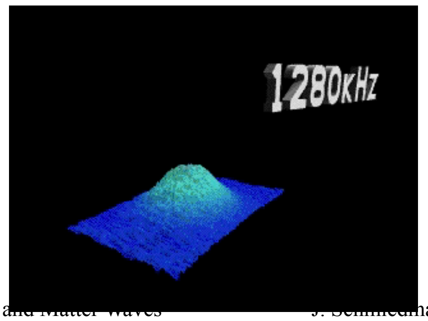

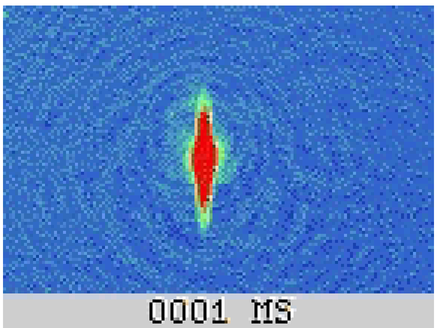

Quantum Degenerate Bose and Fermi Gas

Andrew G. Truscottet al. Science **291**, p2570 (2001)

Bosonen

gehen in den Grundzustand

Fermionen

füllen alle Zustände auf

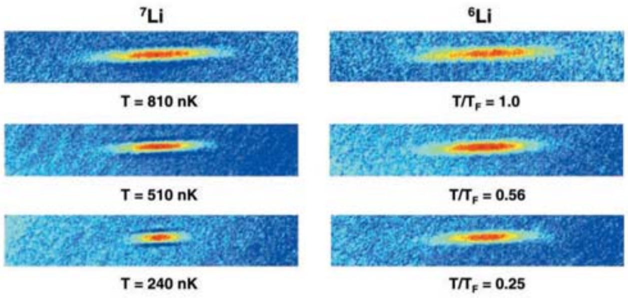

Fig. 1. Two-dimensional false-color images of both ^{7}Li and ^{6}Li clouds. At T/T_F = 1.0, the two clouds are approximately the same size, but as the atoms are cooled further, to T/T_F = 0.56, the Bose gas contracts, whereas the Fermi gas exhibits only subtle changes in size. At T/T_F = 0.25, the size difference between the two gases is clearly discernable. At this temperature the ^{7}Li image displays distortions due to high optical density. However, these distortions are present only in the radial direction and do not affect the measurements. The fitted numbers of ^{7}Li and ^{6}Li atoms, N_7 and N_6, and the fitted temperatures are as follows: For the upper set, N_7 = 2.4 × 10^5, N_6 = 8.7 × 10^4, and T = 810 nK; for the middle set, N_7 = 1.7 × 10^5, N_6 = 1.3 × 10^5, and T = 510 nK; and for the lower set, N_7 = 2.2 × 10^4, N_6 = 1.4 × 10^5, and T = 240 nK. The probe detuning is a parameter of the fits but is constrained to vary by no more than its uncertainty of ±3 MHz. The fits result in typical reduced-χ^2 values of ~1.0. The uncertainties in number and temperature are due mainly to the uncertainties in the fit and are roughly estimated by finding the point at which the reduced-χ^2 increases by 20%. The resulting uncertainties are 8% in temperature and 15% in number. Other sources of uncertainty are relatively insignificant. The size of each displayed image is 1.00 mm in the horizontal axis and 0.17 mm in the vertical axis.

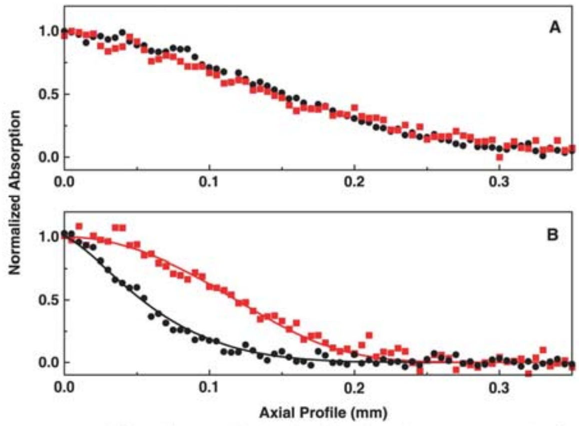

Fig. 2. Comparison of ^{6}Li and ^{7}Li atom cloud axial profiles. The red squares correspond to ^{6}Li, and the black circles to ^{7}Li. (**A**) Data from the top image of Fig. 1, corresponding to T/T_F = 1.0 and T/T_c = 1.5. (**B**) Data from the lower image of Fig. 1, corresponding to T/T_F = 0.25 and T/T_c = 1.0. The fits to the data are shown as solid lines.

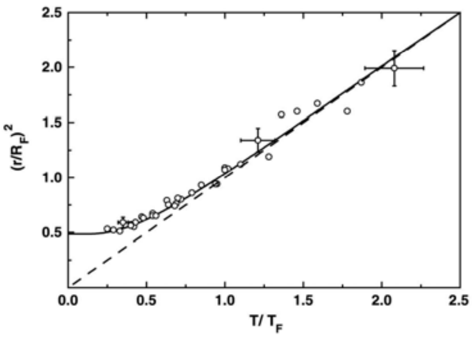

Fig. 3. Square of the 1/e axial radius, r, of the ^{6}Li clouds versus T/T_F. The radius is normalized by the Fermi radius, $R_F = (2k_BT_F/m\omega_a^2)^{1/2}$, where m is the atomic mass of ^{6}Li. The solid line is the prediction for an ideal Fermi gas, whereas the dashed line is calculated assuming classical statistics. The data are shown as open circles. The divergence of the data from the classical prediction is the result of Fermi pressure. Several representative error bars are shown. These result from the uncertainties in number and temperature as described in the legend to Fig. 1. In addition, we estimate an uncertainty of 3% in the determination of r.

VACUUM CHAMBER - REALITY

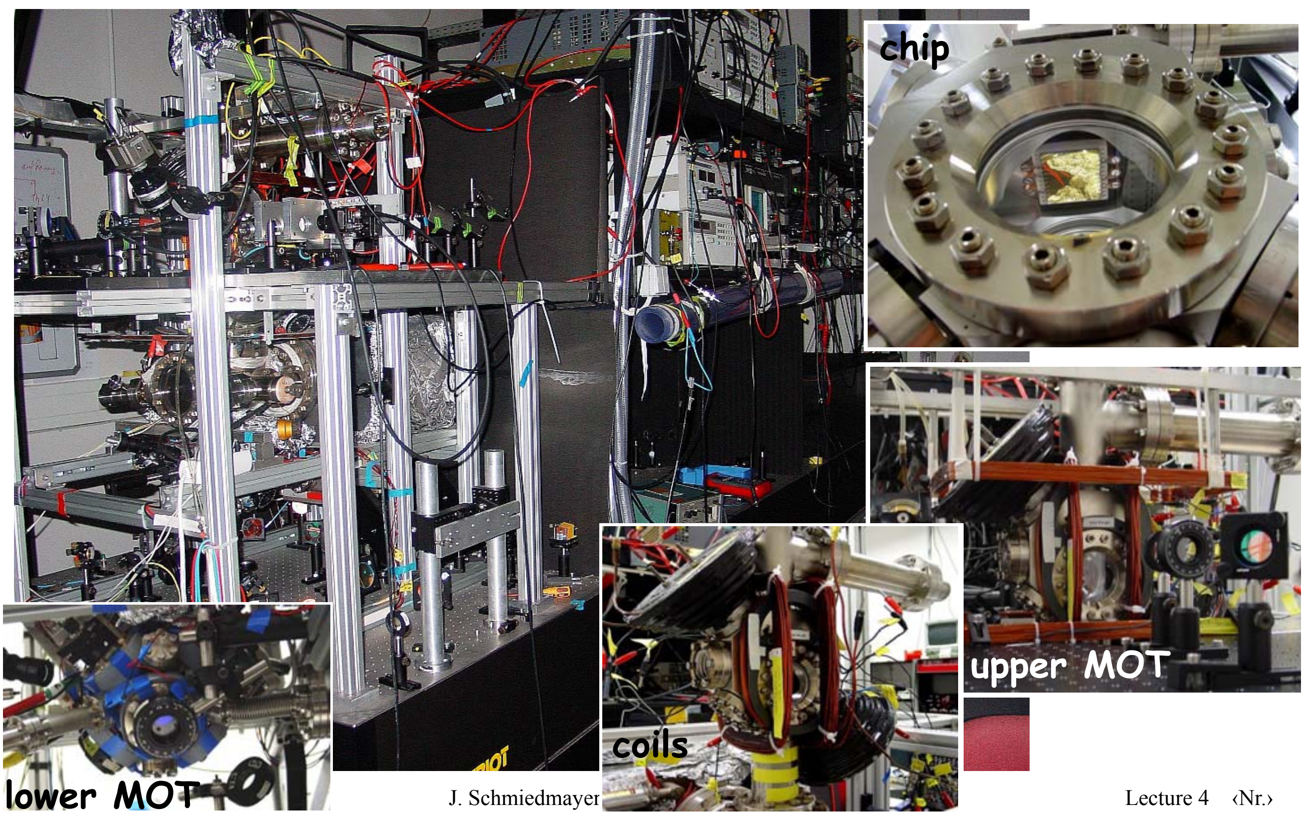

5.3 RF induced adiabatic potentials

Combining static and RF fields

Ioffe-Pritchard trap

$$\begin{aligned} \mathbf{B}_S(\mathbf{r}) &= Gx\mathbf{e}_x - Gy\mathbf{e}_y + B_I\mathbf{e}_z \\ V_{\mathrm{ad}}(r) &= g_F\mu_B F_z\,|\mathbf{B}_S(\mathbf{r})| \\ &= g_F\mu_B m_F\sqrt{G^2\rho^2 + B_I^2} \end{aligned}$$

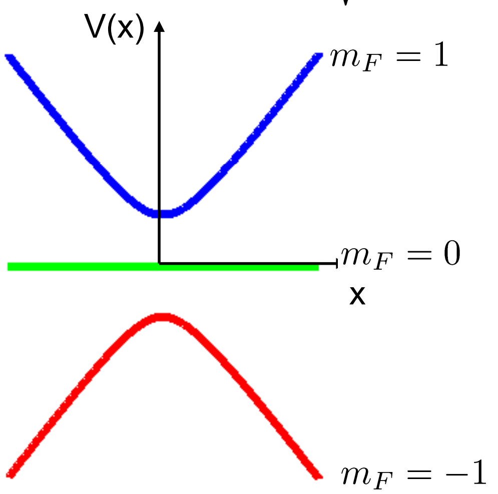

- in a source-free region only mag. field minima are achievable
- number of possible trap shapes can be greatly increased by adding an oscillating RF magnetic field

dressed RF potentials

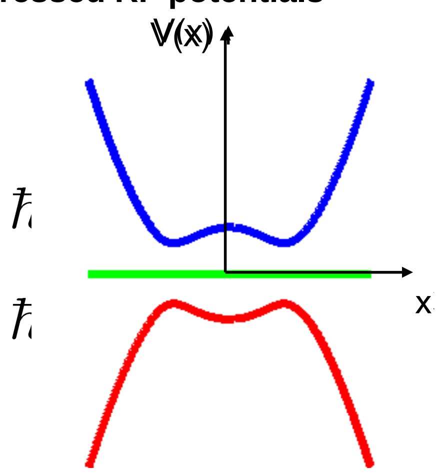

Zobay & Garraway PRL **86**, 1195 (2001)
I. Lesanovsky et al. PRA **73** 033619 (2006)

Dressed adiabatic potentials

Oscillating RF magnetic field

$$\mathbf{B}_{RF}(\mathbf{r},t) = \frac{B_{RF}}{\sqrt{2}}\left[\mathbf{e}_x \cos(\omega t) + \mathbf{e}_y \cos(\omega t + \delta)\right]$$

relative phase shift

Total Hamiltonian

$$H = \frac{\mathbf{p}^2}{2M} + g_F \mu_B \mathbf{F}\cdot\left[\mathbf{B}_S(\mathbf{r}) + \mathbf{B}_{RF}(\mathbf{r},\omega t)\right]$$

1. apply the unitary transformation $U_S(\mathbf{r})$ to diagonalize the static part
2. transform into a rotating frame around the local quantization axis
3. perform the rotating-wave-approximation
4. diagonalize spin-field interaction terms

$$H_{\text{final}} = \frac{1}{2M}\left[\mathbf{p} + \mathbf{A}'(\cancel{\mathbf{r}},t)\right]^2 - \frac{1}{2M}\Phi'(\cancel{\mathbf{r}},t) + \boxed{g_F\mu_B|\mathbf{B}_{\text{eff}}(\mathbf{r})|F_z}$$

adiabatic approximation

dressed adiabatic potentials

B_{eff} does not necessarily obey Maxwell's equations

- potential depends on the relative orientation of the RF and the static field
- spatial dependence gives rise to novel types of RF traps
- free parameter d, i.e. RF polarization can be used to modify the trap shape

theory: I. Lesanovsky et al. PRA **73** 033619 (2006)
I. Lesanovsky et al. PRA **74** 033619 (2006)

experiment: T. Schumm et al. Nature Physics **1**, 57 (2005)
S. Hofferberth et al. Nature Physics **2**, 710 (2006)

RF induced Potentials

state dependent potentials by RF polarization

Polarization of the RF field gives extra freedom

$$\mathbf{B}_S(\mathbf{r}) = Gx\mathbf{e}_x - Gy\mathbf{e}_y + B_I\mathbf{e}_z$$

$$\mathbf{B}_{RF}(\mathbf{r},t) = \frac{B_{RF}}{\sqrt{2}}\left[\mathbf{e}_x \cos(\omega t) + \mathbf{e}_y \cos(\omega t + \delta)\right]$$

$$V_{\text{ad}}(\mathbf{r}) = m_F g_F \mu_B \sqrt{\Omega^2(\mathbf{r}) + \triangle^2(\mathbf{r})}$$

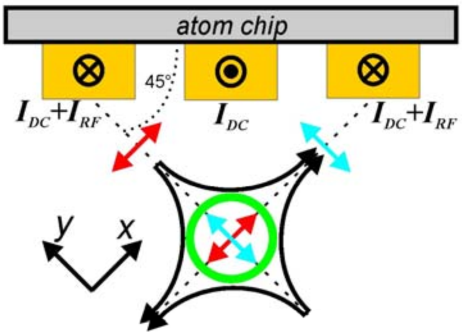

tuning the relative RF phase δ

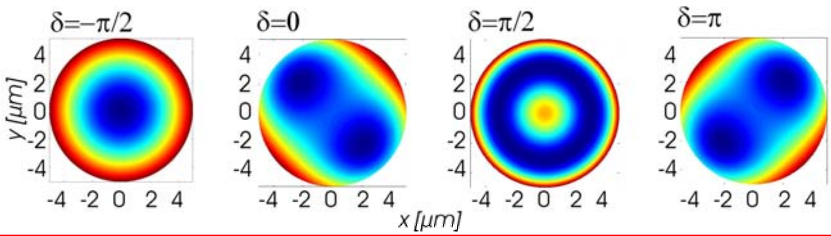

$$\Omega(\mathbf{r}) = |\mathbf{B}_S(\mathbf{r})| - \frac{\hbar\omega}{|g_F\mu_B|}$$

$$\triangle(\mathbf{r}) = \frac{B_{RF}}{2}\left[1 + \frac{B_I \sin\delta_{eff}}{|\mathbf{B}_S(\mathbf{r})|} + \frac{G^2\rho^2}{2\,|\mathbf{B}_S(\mathbf{r})|^2}\left(\cos\delta_{eff}\sin(2\phi) - 1\right)\right]$$

state dependent

$$\boxed{\delta_{eff} = \frac{g_F}{|g_F|}\delta}$$

I. Lesanovsky et al.PRA **73**, 033619 (2006) e-print archive: physics/0510076

RF-Dressed State Potentials
Creating a Double Well

Couple atomic states by RF / MW

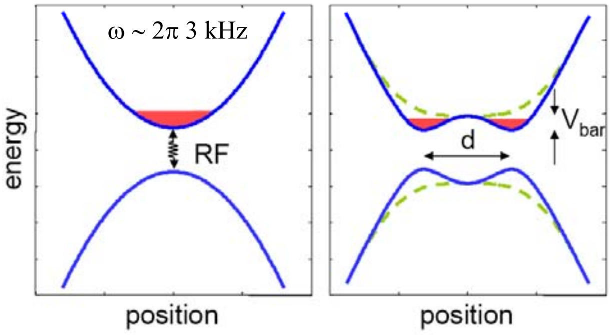

- The minumum of the adiabatic potential is at iso-B surfaces
- The minmum value at the iso-B surface depends on the **RF** couppling strength
- The couppling strength depends on the **orientation** of the RF field relative to the trap field

$$V_{\mathrm{ad}}(\mathbf{r}) = m_F g_F \mu_B \sqrt{\Omega^2(\mathbf{r}) + \triangle^2(\mathbf{r})}$$

realization on AtomChip

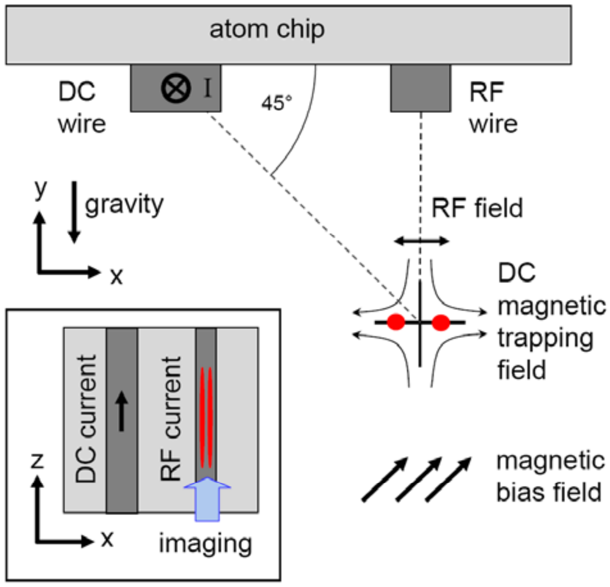

'Matter-wave interferometry in a double well on an atom chip',
T. Schumm, et al., Nature Physics. **1**, 57 (2005)

Observe interference in time of flight

Condensates released from double well fall and expand

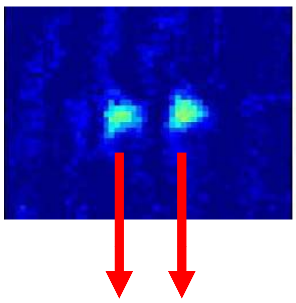

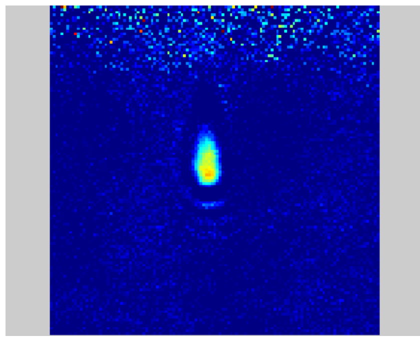

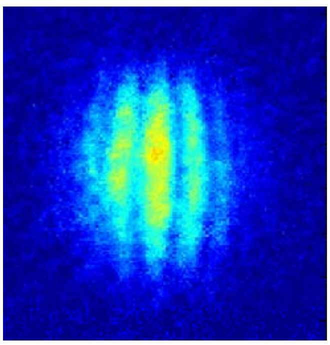

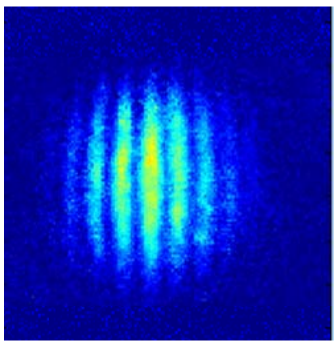

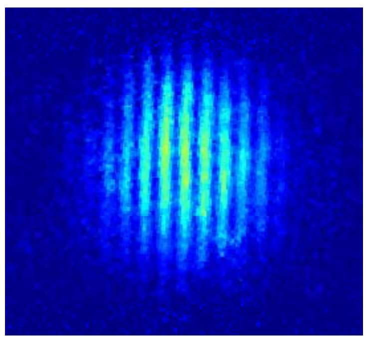

Interference between overlapping BECs

TOF = 16ms

Coherent Splitting

After the BECs has been split far enough to inhibit tunneling (d=3.4 μm), atoms are released and an interference pattern is observed after a time of flight.

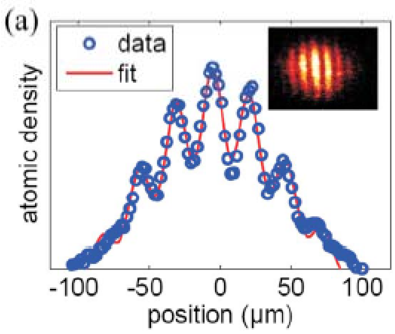

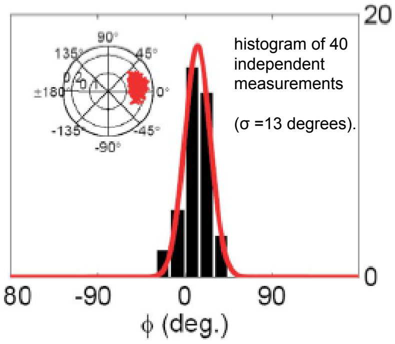

Evolution of the differential phase throughout the splitting process

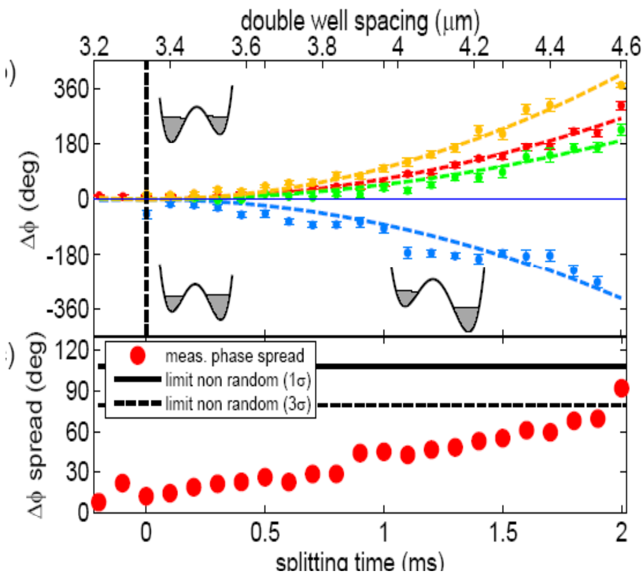

'Matter-wave interferometry in a double well on an atom chip', T. Schumm, et al., Nature Physics. **1**, 57 (2005)

State-dependent double well interference

Demonstration with F=2,m_F=2 state of ^{87}Rb

„effective" polarization depends on g_F

$$\delta_{eff} = \frac{g_F}{|g_F|}\delta$$

RF-potentials allow state-dependant manipulation

elliptical polarization:

state-dependant double well

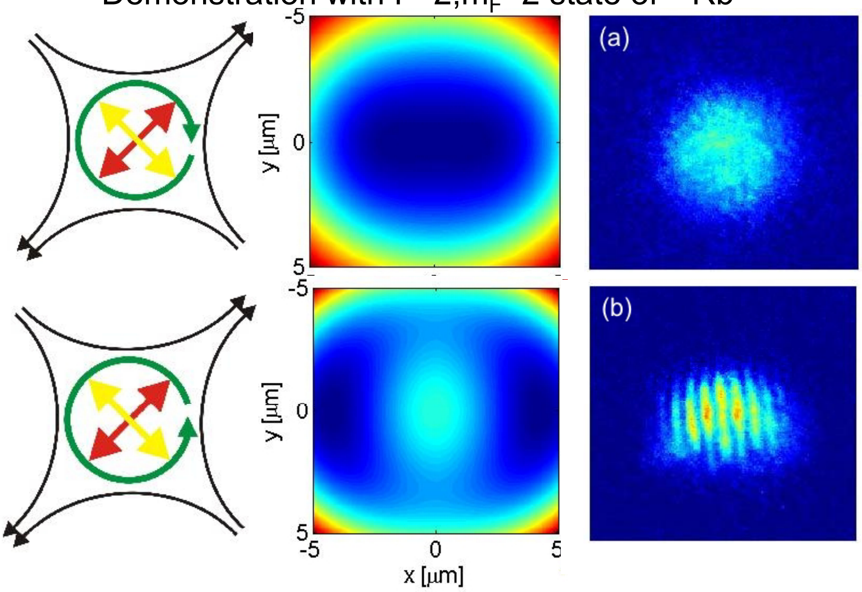

possible application:
collisional phase gate

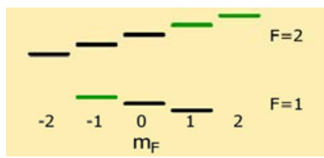

Hofferberth et al. Nature physics Oct. (2006)

Advantages of RF potentials

splitting a trap

Hoffererth et al. Nature Physics 2, 710 (2006)

- True spliting 1 trap -> 2 traps
  - Confinement in transvrsal direction stays the same
  - Confinement in splitting direction is significantly tighter
- splitting potential: $V(x)=A(t)\,x^2+\mathbf{B}\,x^4$
  the size of the x^4 term determines the confinement
  In RF potentials **B** is factor ~1000 larger

2-wire beam splitter

contours 5 Hz

RF beam splitter

contours 5 kHz

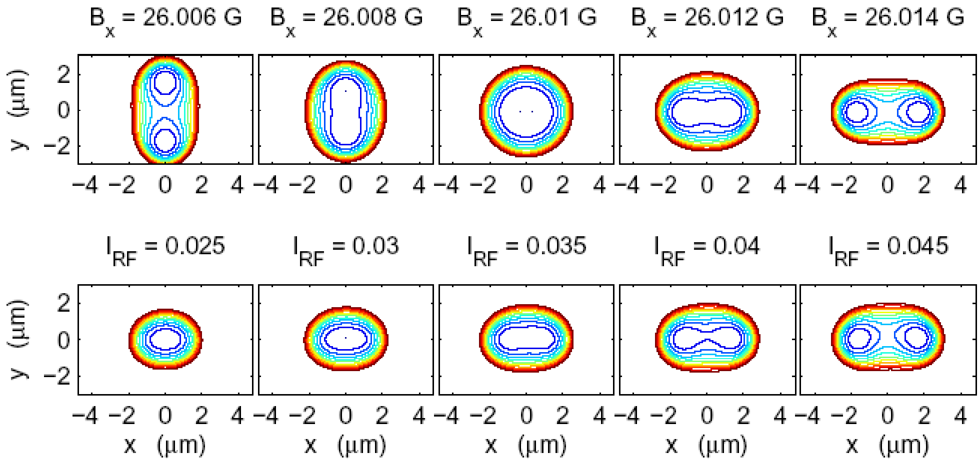

RF and MW induced adiabatic potentials

create adiabatic dressed state potentials by coupling electronic ground states of an atom

- coupling between stable states allows to create conservative potentials even with on resonant radiation
- shaping the potential:
  - detuning the states with an external magnetic field
  - spatial dependent coupling strength (RF field)
    -> allows strong field seeker traps
- coupling is magnetic:
  the amplitude and the relative orientation of the RF field and the detuning field are important

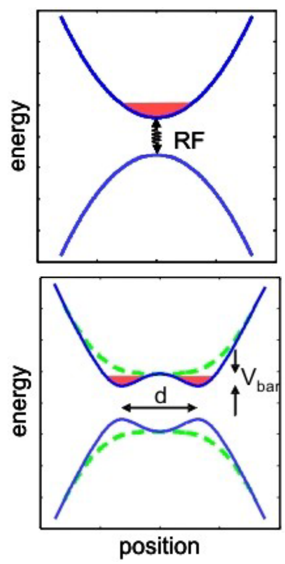

- first experiment: dressed neutrons: E. Muskat et al., PRL **58**, 2047 (1987).
- first proposal of a MW trap (detuned) C. Agosta, et al. PRL. **62**, 2361 (1989).
- MW experiment (Cs, detuned) R. Spreeuw, et al. PRL **72**, 3162 (1994).
- RF dressed state traps O. Zobay, B. M. Garraway, PRL **86**, 1195 (2001).
  (with magnetic field detuning but neglecting polarization)
- RF potentials for thermal Rb atoms: Y. Colombe, et al. Europhys. Lett. **67**, 593 (2004).
- Full implementation T. Schumm et al Nature Physics **1**, 57 (2005)

RF and MW induced state dependent potentials

The two clock states have

$|F=2, m_F=1\rangle$

$|F=1, m_F=-1\rangle$

- Identical Zeeman shift
- Identical Stark shift
- Identical light shift (for large detuning)

Radio Frequency (RF) and Micro Wave (MW) fields can couple differently

On chip: local RF and MW field for manipulaion

Linear polarized micro wave

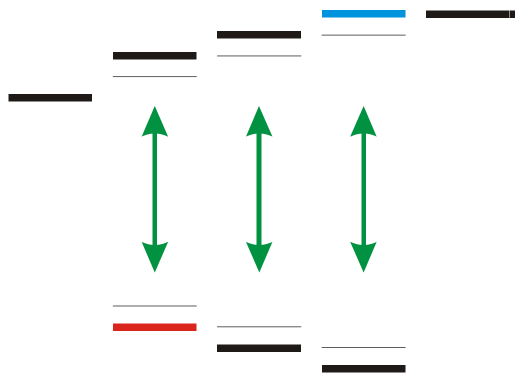

AC-Zeeman shift:

$$\Delta E = \pm \frac{\hbar\Omega_R^2}{4\Delta}, \quad \text{with} \ (|\Delta| >> \Omega_R)$$

$$\hbar\Omega_R \sim \mu_B \cdot B_{MW}$$

M. Cirone et al. quant-ph/0505194 (EPJ D special issue atom chip)
RF idea: M. Anderson (HD)